Synthetic exceptional points and unidirectional zero reflection in non-Hermitian acoustic systems

Chen Shen, Junfei Li, Xiuyuan Peng, and Steven A. Cummer*
Department of Electrical and Computer Engineering, Duke University, Durham, North Carolina 27708, USA

(Received 31 August 2018; published 17 December 2018)

Exceptional points (EPs) are responsible for a number of interesting phenomena in non-Hermitian wave systems. Here we show, both theoretically and experimentally, that EPs can be synthesized in non-Hermitian acoustic systems with unbalanced loss factors in different sections. Numerical simulations and measurements confirm that unidirectional zero reflection, one of the hallmarks of EPs, can be realized in such a compact system with controlled Willis coupling and loss. When approached from one direction in the parameter space, the material slab mimics a conventional parity-time (PT) symmetric system. Our findings provide an efficient way for advanced engineering of scattering properties of artificial acoustic materials with EP-related physics.

DOI: 10.1103/PhysRevMaterials.2.125203

I. INTRODUCTION

The emergence of exceptional points (EPs) in non-Hermitian systems has stimulated extensive research interest in recent years [1–3]. In a two-level system, EPs mark the spontaneous symmetry-breaking transition point in which the energy spectrum jumps from real to complex value abruptly [3–5]. This type of phase transition exists in non-Hermitian Hamiltonians and is responsible for a number of useful and unexpected phenomena. Although EPs were originally analyzed in the realm of quantum mechanics, they have attracted research effort in other regimes as well, thanks to the mathematical equivalence between Schrödinger equation and paraxial electromagnetic wave equations. To date, EPs have been studied in various physical systems, including optics [6–9], photonics [10–13], acoustics [14–18], and others [19–21]. Numerous intriguing applications have been demonstrated within the context of EPs, such as unidirectional invisibility [9,15], single-mode or vortex lasers [22–24], enhanced sensing [25,26], and topological effects [27–29].

Physical realizations of EPs generally fall into two categories. The first approach is to use PT-symmetric synthetic media, in which the constitutive components are patterned so that the entire system display an exact balanced loss and gain. Such PT-symmetric media typically involve wave amplification/absorption materials or structures and precise control of their spatial variation for the access of the whole complex parameter domain to respect PT symmetry. The lack of easily controllable gain media also poses additional challenges on the fabrication of a PT-symmetric medium, as an external energy supply or a means of field control are required. Although entirely passive PT-symmetric media have been proposed [9,30], a continuous varying loss profile is demanded which inevitably adds to the system complexity.

The other approach to realize EPs uses coupled systems such as resonators, cavities, or waveguides. Although these systems exhibit EPs in a compact implementation, they require relatively sophisticated design and carefully controlled loss within the system. The coupling strength and additional loss, which are critical for the synthesis of EPs, may be unstable under small perturbations and are difficult to control precisely in practice. These requirements make EPs difficult to access physically, limiting their use in practical applications.

A necessary condition for the formation of EPs is the coalescence of the eigenstates of the scattering matrix, which requires $|r^+| \neq |r^-|$. This means that the system should exhibit a directionally dependent response under different excitations. Bianisotropic media are possible candidates to realize such asymmetric responses. The term bianisotropy originates from electromagnetism [31] and the concept is the direct analog to Willis coupling [32] in acoustics and elastodynamics, in which a cross coupling between strain and velocity takes place. Recent studies have shown that bianisotropic acoustic media can lead to asymmetric responses [33–37]. However, they are generally designed to be lossless and thus obey $|t^\pm|^2 + |r^\pm|^2 = 1$, in which $t^\pm$ and $r^\pm$ are the local transmission and reflection coefficients in the forward and backward directions, respectively. As $t^+ = t^-$ for reciprocal systems, the amplitudes of the local reflection coefficients are the same, i.e., $|r^+| = |r^-|$. Therefore, lossless bianisotropic structures do not have access to EPs and are not suitable for unidirectional scattering manipulation with different amplitudes.

In this paper we show that EPs can be systematically synthesized in bianisotropic non-Hermitian acoustic systems with engineered loss. When loss is carefully incorporated into the system, unidirectional zero reflection, i.e., vanishing reflection in only one direction of illumination, can be realized in the all-passive structure. This property is a result of degenerate non-Hermitian scattering matrix at the EP of the system. Distinct from conventional PT-symmetric systems where loss and gain need to be judiciously tailored, the EPs proposed here can be synthesized conveniently by adding appropriate loss into the host medium of the system. Moreover, no continuous variation of loss is required for the synthesis of EPs. Such compact, entirely passive structure can serve as a versatile platform to engineer scattering properties and explore EP-related physics.

*Corresponding author: cummer@ee.duke.edu

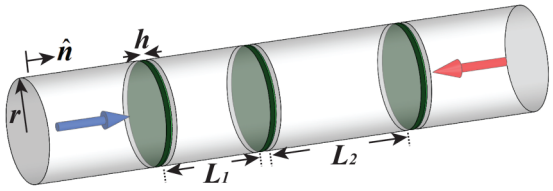

FIG. 1. Sketch of the bianisotropic system composed of three thin plates and two lossy medium regions. All the components are loaded in a circular waveguide to ensure 1D wave propagation. The arrows indicate incident acoustic waves from different directions.

II. THEORY AND DESIGN

To begin with, we consider an asymmetric structure as shown in Fig. 1. The structure consists of two lossy medium regions and is loaded in a circular waveguide. Thin plates are connected at the termination of each region. The lengths of the two regions are L_1 and L_2, respectively and are not equal. Such a structure lacks inversion symmetry and therefore exhibits bianisotropic response. It is worth pointing out that, to realize unidirectional scattering properties, asymmetry is essential since the behavior of a symmetrical structure is the same regardless of the direction of incidence. It has been shown that for a lossless and reciprocal system, the amplitudes of the reflection coefficients when illuminated on two sides are identical [36]. In order to obtain different reflection amplitudes, loss is introduced as another ingredient so that the system becomes non-Hermitian. To do this, loss factors δ_1 and δ_2 are assumed in the two medium regions and the wave number k_i inside the medium becomes $k_i = k_0(1 - j\delta_i)$, where k_0 is the free space wave number. While the impedances of the plates can generally be different to allow arbitrary bianisotropic response [33,36,38], here they are considered identical for simplicity and we will show that the geometrical asymmetry and unbalanced loss factors are sufficient for the synthesis of EPs.

The system can be analyzed by the standard two-port network model as below:

$$\begin{bmatrix} p_{\text{in}} \\ -\hat{n}\cdot\vec{v}_{\text{in}} \end{bmatrix} = \begin{bmatrix} A & B \\ C & D \end{bmatrix} \begin{bmatrix} p_{\text{out}} \\ -\hat{n}\cdot\vec{v}_{\text{out}} \end{bmatrix}. \tag{1}$$

Here p_{in} and p_{out} represent the input and output complex pressure amplitudes at the two terminals of the structure, $\hat{n}$ is the normal vector of the wave propagation direction, and $\vec{v}_{\text{in}}$ and $\vec{v}_{\text{out}}$ are the associated input and output velocity fields. The total transfer matrix is expressed as

$$\begin{bmatrix} A & B \\ C & D \end{bmatrix} = M_{\text{Z}} M_{\text{T1}} M_{\text{Z}} M_{\text{T2}} M_{\text{Z}}. \tag{2}$$

M_{Z} and M_{Ti} are the transfer matrices of the plate (regarded as an impedance Z_s) and the lossy medium, respectively, and are expressed as

$$M_{\text{Z}} = \begin{bmatrix} 1 & Z_s \\ 0 & 1 \end{bmatrix}, \tag{3}$$

$$M_{\text{Ti}} = \begin{bmatrix} \cos(k_i L_i) & jZ_0 \sin(k_i L_i) \\ j\frac{1}{Z_0}\sin(k_i L_i) & \cos(k_i L_i) \end{bmatrix}, \tag{4}$$

where $Z_0 = \rho_0 c_0$ is the characteristic impedance of the background medium (air in our study), with ρ_0 and c_0 being the density and speed of sound in air. Generally Z_0 will be a complex number by the introduction of loss, however, its absolute value change is small and the resulting impedance mismatch is therefore negligible. We note that the plates serve as impedance sheets in the transmission line system, and they can be replaced by other structures that can be regarded as an impedance, e.g., side-loaded Helmholtz resonators. Here we chose to use paper plates for the sake of the compactness of the system. The corresponding S matrix of the system can be derived as (note that the S matrix here is different from its conventional form in electromagnetics [39,40])

$$S = \begin{bmatrix} t^- & r^- \\ r^+ & t^+ \end{bmatrix} = \begin{bmatrix} \frac{2}{A+B/Z_0+CZ_0+D} & \frac{-A+B/Z_0-CZ_0+D}{A+B/Z_0+CZ_0+D} \\ \frac{A+B/Z_0-CZ_0-D}{A+B/Z_0+CZ_0+D} & \frac{2}{A+B/Z_0+CZ_0+D} \end{bmatrix}. \tag{5}$$

To this end, the components of the S matrix of the system are first calculated by inserting Eqs. (3) and (4) into Eq. (5) and varying δ_1 and δ_2 in the parameter space. Without loss of generality, Z_s is set to be $i620\,\text{Pa}\cdot\text{s/m}$, which is purely imaginary. This condition can be satisfied if the plates are thin and elastic and can be considered lossless. The value is chosen such that it is moderate compared to Z_0 ($Z_s = 1.46iZ_0$) and is therefore conveniently attainable for plate-type metamaterials [41]. On the other hand, as will be shown later, this Z_s will lead to a reasonable set of δ_1 and δ_2 values that need to be realized in experiments to induce EPs. The frequency of the incident wave is chosen to be 2.95 kHz for the convenience of experimental realization. Operation at other frequencies can be achieved simply by changing the geometrical configuration of the system such that the plates have desired impedance. Figures 2(a)–2(c) depict the calculated absolute values of r^+, r^-, and $t^+(t^-)$ against the two control parameters δ_1 and δ_2, with fixed lengths $L_1 = 20$ mm and $L_2 = 30$ mm. The local reflectance display different characteristics while the transmittance is identical in both directions. This is because the system is linear time invariant and does not break the reciprocity. Unidirectional zero reflection, i.e., $r^+ = 0$ and $r^- \neq 0$, occurs when $\delta_1 = 0.02$ and $\delta_2 = 0.22$.

To confirm that this operation point is truly an EP, we further calculate the eigenvalues of the S matrix $\lambda_{1,2} = t \pm (r^+r^-)^{1/2}$ (here $t = t^+ = t^-$) by setting $\delta_1 = 0.02$ and increasing δ_2 monotonically. As can be seen from Figs. 2(d) and 2(e), at $\delta_2 = 0.22$, there is a coalescence of the real part of the eigenvalues and the imaginary part experiences biased distributions when $\delta_2 > 0.22$. The absolute values of $\lambda_{1,2}$ shown in Fig. 2(f) undergo a phase transition at this point and the two eigenstates become degenerate. Such an eigenvalue spectrum is quite similar to the behavior of a PT-symmetric system that is experiencing a change from PT-exact phase to PT-broken phase at the EP. Interestingly, the eigenvalues are not unimodular at the EP compared with balanced PT-symmetric systems. This is similar to a passive PT-symmetric system in which the eigenvalues are offset by the introduction of losses [30].

It should be pointed out that although δ_1 is not zero, the system can still possess EPs if medium 1 is entirely lossless (i.e., $\delta_1 = 0$). In other words, in our transmission-line system, the additional tuning of δ_1 is not required in order to form an

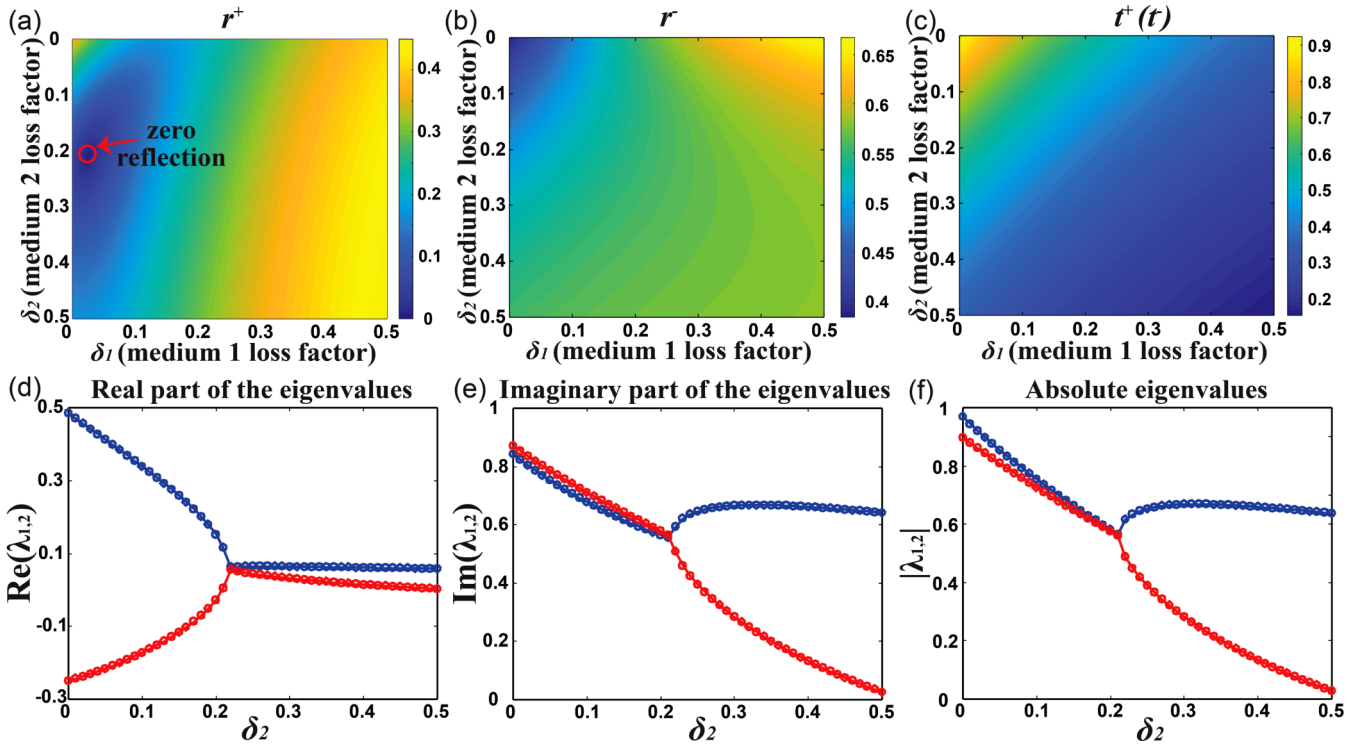

FIG. 2. Characteristics of the non-Hermitian acoustic system. (a)–(c) Scattering parameters of the system in the parameter space $\delta_{1,2}$. The reflection coefficients r^+ and r^- show distinctive behavior, which is a clear signature of asymmetric response. The arrow marks unidirectional zero reflection, which occurs for $\delta_1 = 0.02$ and $\delta_2 = 0.22$. (d) Real and (e) imaginary part of the eigenvalues in the parameter space. The eigenvalues are plotted as a function of δ_2 by fixing $\delta_1 = 0.02$. (f) Absolute eigenvalues of the corresponding S matrix.

EP. Medium 1 can generally be either lossless or lossy and only δ_2 is important in the parameter space so that an EP appears. Here it is chosen to have a finite value to represent a typical loss in the experimental environment. The corresponding Z_s for the emergence of an EP with only one lossy medium (medium 2) can be calculated by enforcing $\delta_1 = 0$ and $r^+ = 0$, which is found to be $i580\,\mathrm{Pa}\cdot\mathrm{s/m}$. Likewise, an EP can also be achieved by keeping $\delta_2 = 0$ and varying δ_1. Since the only parameter that needs to be tuned is δ_2, the proposed scheme here using bianisotropic non-Hermitian system greatly facilitates the synthesis of an EP.

To fully design the physical system, the radius r of the circular waveguide must be determined such that the paper plates display the desired impedance. The acoustic impedance of the plates with clamped boundaries can be computed by a lumped model described by acoustic compliance C_a and acoustic mass M_a [41,42]:

$$Z_{\mathrm{a}} = \frac{1}{j\omega C_a} + j\omega M_a. \tag{6}$$

For circular plates, the values can be approximated by $M_a = 1.8830\frac{\rho_p h}{\pi r^2}$ and $C_a = \frac{\pi r^6}{196.51D}$, where ρ_p, h, and D are the density, thickness, and flexural rigidity of the plate, respectively. The characteristic impedance Z_s of the plate is therefore $Z_s = Z_a A$ with $A = \pi r^2$ being the surface area of the plate. For the plates we use in the study, the density and thickness are 728 $\mathrm{kg/m^3}$ and 0.26 mm, respectively. The flexural rigidity is determined by measuring the transmission spectrum of a single plate [43]. For a circular plate with clamped boundaries, the flexural rigidity is given by [44]

$$D = 0.0383 f_0^2 A^2 \rho_p h, \tag{7}$$

where f_0 is the first resonance frequency of the plate. Figure 3 shows the measured transmission coefficient through a single paper plate with $r = 10$ mm. The peak frequency is 2.81 kHz, with transmission coefficient being greater than 0.9, which justifies the assumption of low loss of the paper plates around resonance frequencies. From Eq. (7), the flexural rigidity of

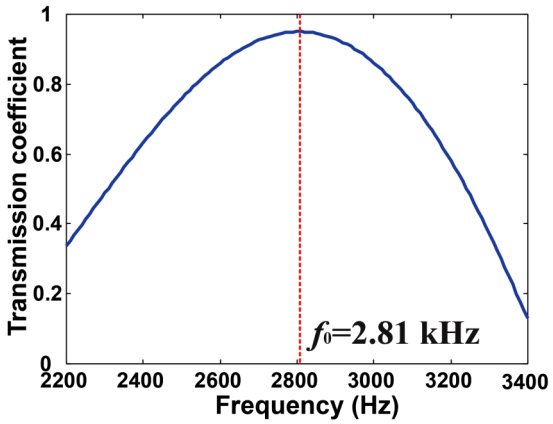

FIG. 3. Experimentally measured transmission spectrum through a single paper plate with clamped boundaries. The first resonance frequency (corresponds to a transmission peak) is found to be $f_0 =$ 2.81 kHz.

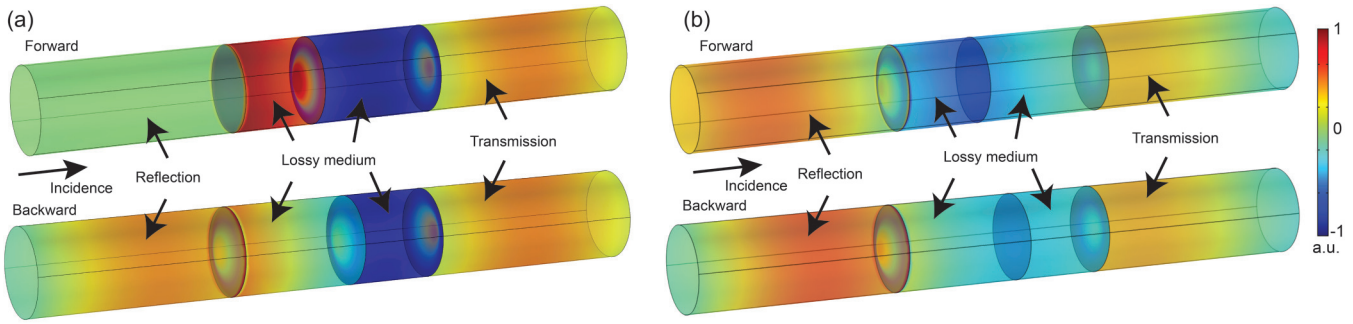

FIG. 4. Simulated sound pressure distribution and mode shape of the plates of the non-Hermitian acoustic system. The incident waves are omitted for better visualization of the reflected waves. Top and bottom panels show the forward and backward incidence, respectively. (a) Response at the designed frequency 2.95 kHz, with zero reflection in the forward direction. (b) Response at a slightly higher frequency 3.00 kHz, the reflection in both directions has a finite value.

the plates is found to be 0.0057 Pa · m^4. The calculated radius r of the plate according to Eq. (6) is 10 mm so that $Z_s = i620$ Pa · s/m at 2.95 kHz, and is used in the following section for numerical simulations and experiments.

III. SIMULATION AND MEASUREMENTS

Full-wave simulations are performed with the finite element solver COMSOL Multiphysics. The pressure acoustic module and solid mechanics module are used so that both lossy medium and plates can be fully modeled. The acoustic pressure distribution and mode shapes of the plates are shown in Fig. 4 at 2.95 and 3.00 kHz. It can be seen that for incoming waves in opposite directions, the reflected pressure fields display vastly different characteristics at the designed operational frequency 2.95 kHz. The reflection in the forward direction is almost zero, which agrees well with theoretical predictions. When the incident frequency is increased to 3.00 kHz, the reflection increases in the forward direction. On the other hand, the acoustic pressure distributions on the transmission are identical for both frequencies in terms of amplitude and phase since the system does not break reciprocity.

To experimentally demonstrate unidirectional zero reflection with the bianisotropic system, a prototype is constructed with the configuration described and simulated above. The experimental setup is shown in Fig. 5(a). The tubes are three-dimensionally (3D) printed using nylon whose impedance is much greater than air and can be considered acoustically rigid. The thickness of the tubes is 5 mm to ensure one-dimension (1D) wave propagation. The plates are rigidly clamped between adjacent sections of the tubes and a speaker with 0.9 cm radius and 4 Ohm input impedance is positioned at one end of the tube. The speaker is powered by an amplifier (type PAM8403) and generates acoustic waves to excite the system.

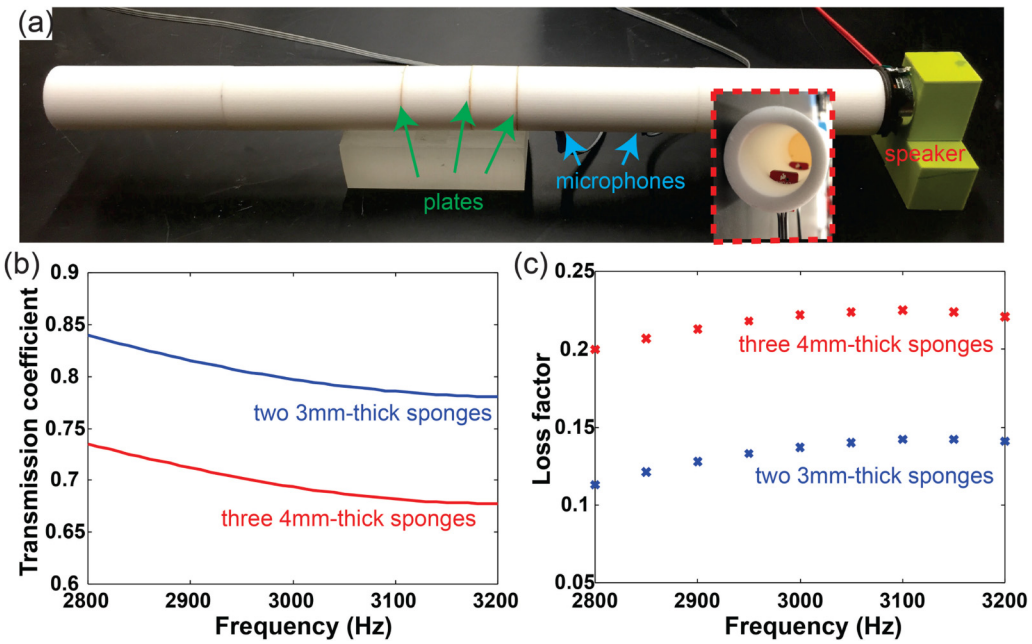

FIG. 5. (a) Experimental setup for reflection measurement. Two microphones are inserted into the tube to capture the incident and reflected signals. The inset shows how the microphones are positioned inside the tube. (b) Measured transmission coefficient and (c) retrieved loss factor of the 3 cm lossy medium.

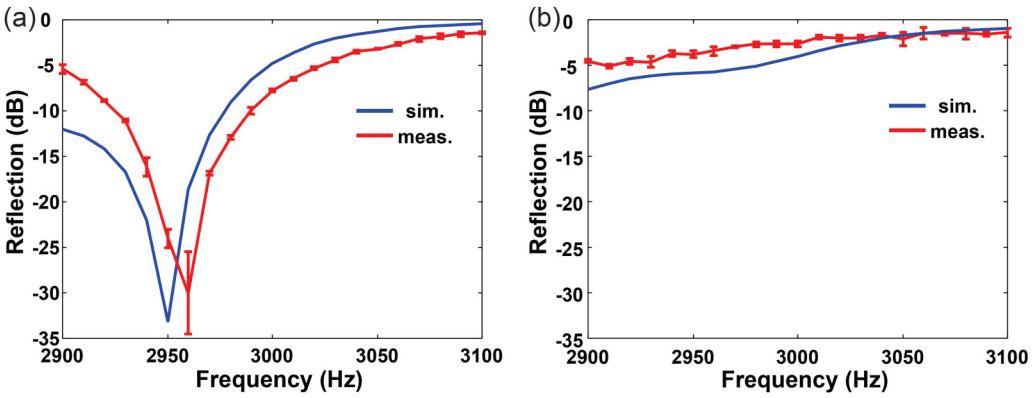

FIG. 6. Experimental demonstration of unidirectional zero reflection of the non-Hermitian acoustic system. Measured and simulated reflection spectrum in the (a) forward and (b) backward directions. The error bars are generated out of six measurements.

To measure the reflection of the sample, two breakout boards (type ADMP401) are mounted inside the tube with a distance of 4 cm. The breakout boards have a size of 13.6 mm by 10.4 mm and feature a 1.2 mm diameter MEMS microphone on the tip. The boards are slid into the tube through a slit such that only the tip is inserted into the tube to ensure minimal contact with the field [see the inset of Fig. 5(a)]. The microphones are oriented on the same side in front of the sample and the signals are recorded and data acquisition is performed using NI board PCI-6251 and CB-68LP as the interface. The reflectivity is extracted via the standard two-microphone method [45]. The direction of incident waves is then switched to obtain the response of the other direction. Six individual measurements are averaged to reduce noise.

The loss factors of the two medium sections are first determined so that they display theoretically required values. For lossy medium 1, its loss factor $\delta_1 = 0.02$ represents a typical loss in the experimental environment and therefore no additional tailoring is applied [46]. On the other hand, for lossy medium 2, a suitable amount of additional loss should be introduced so that its loss factor reaches 0.22. To do this, several equally spaced disklike pieces of sponges [47] are inserted inside the tube. The radius of the sponges is identical to the inner radius of the tube r so that an effectively uniform lossy region can be created. The loss factor can be adjusted by varying the number and thickness of the sponges that are used. Since the sponges are dissipative to acoustic waves, higher loss factors can be obtained by monotonically increase the overall sponge thickness that is inserted in the tube until the requirement is met [48]. To show the tunability of the lossy medium using sponges, we measure the transmission coefficient of medium 2 with different configurations of sponges and the results are depicted in Fig. 5(b). The blue and red curves represent the cases of using two 3-mm-thick and three 4-mm-thick sponges, respectively. Clearly the transmission coefficient decreases with more and thicker sponges added. We further calculate the corresponding loss factors of the medium using the transfer matrix method. Figure 5(c) shows the calculated loss factors of the two cases. The retrieved loss factors are a little dispersive and are slightly larger at higher frequencies, which is typical for sound absorbing sponges. The retrieved loss factor is roughly 0.22 around the operational frequency (2.95 kHz) and corresponds to the case used in the study.

Figures 6(a) and 6(b) show the measured reflection spectra of the sample in the forward and backward directions. Good agreement is observed between the simulated results and measurements. The small discrepancies can be attributed to the slight nonuniformity of the paper plates and weak scattering caused by the microphones. The operational frequency for unidirectional zero reflection is slightly shifted from 2.95 to 2.96 kHz in experiments, which can be caused by nonideal performance of the plates due to imperfect boundary conditions and small material loss. The non-Hermitian bianisotropic system shows distinctly different reflection characteristics in opposite directions, indicating unidirectional scattering properties. At 2.95 kHz, the reflectivity in the forward direction approaches -30 dB in both simulations and experiments, while reflectivity in the backward direction is much larger and near -5 dB in measurement. This clearly illustrates exceptional point behavior of the system.

IV. CONCLUSIONS

To conclude, we have shown both theoretically and experimentally that a non-Hermitian bianisotropic acoustic system can exhibit the exceptional point behavior of much more complicated PT-symmetric systems. The constraint of balanced loss and gain can be relaxed for the synthesis of EPs in such a material slab. Unidirectional zero reflection, a key property of PT-symmetric systems, can be realized by adding modest loss to the constitutive medium of an appropriately designed system. The bianisotropy and non-Hermiticity add a new degree of freedom to the system design and it is shown that they can contribute to strongly asymmetric scattering properties. Although such EPs are demonstrated in the acoustic regime, the theory is not restricted to acoustics and can easily be extended to other scenarios such as microwaves. For example, the plates can be replaced by impedance sheets and the lossy medium can be realized by materials with certain dielectric loss. The size of the structure in our study is less than half of the operational wavelength and can be reduced by further optimization. The structure is also able to be integrated into two dimensions in the lateral direction to

form a metasurface. The bianisotropic non-Hermitian systems demonstrated here can serve as a simple platform for the exploration and realization of EP-related physics and can thus find applications in directional sensing and communication, unidirectional invisibility, and other areas without the need for more complicated full PT-symmetric systems.

ACKNOWLEDGMENTS

This work was supported by the Multidisciplinary University Research Initiative grant from the Office of Naval Research (Grant No. N00014-13-1-0631) and an Emerging Frontiers in Research and Innovation grant from the National Science Foundation (Grant No. 1641084).

[1] C. M. Bender and S. Boettcher, Phys. Rev. Lett. **80**, 5243 (1998).

[2] C. M. Bender, D. C. Brody, and H. F. Jones, Phys. Rev. Lett. **89**, 270401 (2002).

[3] C. M. Bender, Rep. Prog. Phys. **70**, 947 (2007).

[4] L. Feng, R. El-Ganainy, and L. Ge, Nat. Photon. **11**, 752 (2017).

[5] R. El-Ganainy, K. G. Makris, M. Khajavikhan, Z. H. Musslimani, S. Rotter, and D. N. Christodoulides, Nat. Phys. **14**, 11 (2018).

[6] A. Guo, G. J. Salamo, D. Duchesne, R. Morandotti, M. Volatier-Ravat, V. Aimez, G. A. Siviloglou, and D. N. Christodoulides, Phys. Rev. Lett. **103**, 093902 (2009).

[7] C. E. Rüter, K. G. Makris, R. El-Ganainy, D. N. Christodoulides, M. Segev, and D. Kip, Nat. Phys. **6**, 192 (2010).

[8] Z. Lin, H. Ramezani, T. Eichelkraut, T. Kottos, H. Cao, and D. N. Christodoulides, Phys. Rev. Lett. **106**, 213901 (2011).

[9] L. Feng, Y.-L. Xu, W. S. Fegadolli, M.-H. Lu, J. E. Oliveira, V. R. Almeida, Y.-F. Chen, and A. Scherer, Nat. Mater. **12**, 108 (2013).

[10] A. Regensburger, C. Bersch, M.-A. Miri, G. Onishchukov, D. N. Christodoulides, and U. Peschel, Nature (London) **488**, 167 (2012).

[11] Y. Lumer, Y. Plotnik, M. C. Rechtsman, and M. Segev, Phys. Rev. Lett. **111**, 263901 (2013).

[12] B. Peng, Ş. K. Özdemir, F. Lei, F. Monifi, M. Gianfreda, G. L. Long, S. Fan, F. Nori, C. M. Bender, and L. Yang, Nat. Phys. **10**, 394 (2014).

[13] M. Lawrence, N. Xu, X. Zhang, L. Cong, J. Han, W. Zhang, and S. Zhang, Phys. Rev. Lett. **113**, 093901 (2014).

[14] X. Zhu, H. Ramezani, C. Shi, J. Zhu, and X. Zhang, Phys. Rev. X **4**, 031042 (2014).

[15] R. Fleury, D. Sounas, and A. Alù, Nat. Commun. **6**, 5905 (2015).

[16] C. Shi, M. Dubois, Y. Chen, L. Cheng, H. Ramezani, Y. Wang, and X. Zhang, Nat. Commun. **7**, 11110 (2016).

[17] J. Christensen, M. Willatzen, V. R. Velasco, and M.-H. Lu, Phys. Rev. Lett. **116**, 207601 (2016).

[18] V. Achilleos, G. Theocharis, O. Richoux, and V. Pagneux, Phys. Rev. B **95**, 144303 (2017).

[19] H. Cartarius and G. Wunner, Phys. Rev. A **86**, 013612 (2012).

[20] D. Dast, D. Haag, H. Cartarius, and G. Wunner, Phys. Rev. A **90**, 052120 (2014).

[21] V. V. Konotop, J. Yang, and D. A. Zezyulin, Rev. Mod. Phys. **88**, 035002 (2016).

[22] L. Feng, Z. J. Wong, R.-M. Ma, Y. Wang, and X. Zhang, Science **346**, 972 (2014).

[23] H. Hodaei, M.-A. Miri, M. Heinrich, D. N. Christodoulides, and M. Khajavikhan, Science **346**, 975 (2014).

[24] P. Miao, Z. Zhang, J. Sun, W. Walasik, S. Longhi, N. M. Litchinitser, and L. Feng, Science **353**, 464 (2016).

[25] W. Chen, Ş. K. Özdemir, G. Zhao, J. Wiersig, and L. Yang, Nature (London) **548**, 192 (2017).

[26] H. Hodaei, A. U. Hassan, S. Wittek, H. Garcia-Gracia, R. El-Ganainy, D. N. Christodoulides, and M. Khajavikhan, Nature (London) **548**, 187 (2017).

[27] S. Malzard, C. Poli, and H. Schomerus, Phys. Rev. Lett. **115**, 200402 (2015).

[28] L. Xiao, X. Zhan, Z. Bian, K. Wang, X. Zhang, X. Wang, J. Li, K. Mochizuki, D. Kim, N. Kawakami *et al.*, Nat. Phys. **13**, 1117 (2017).

[29] S. Weimann, M. Kremer, Y. Plotnik, Y. Lumer, S. Nolte, K. Makris, M. Segev, M. Rechtsman, and A. Szameit, Nat. Mater. **16**, 433 (2017).

[30] T. Liu, X. Zhu, F. Chen, S. Liang, and J. Zhu, Phys. Rev. Lett. **120**, 124502 (2018).

[31] I. V. Lindell, A. Sihvola, S. Tretyakov, and A. Viitanen, *Electromagnetic Waves in Chiral and Bi-isotropic Media* (Artech House, London, 1994).

[32] G. W. Milton and J. R. Willis, Proc. R. Soc. London Ser. A **463**, 855 (2007).

[33] S. Koo, C. Cho, J.-h. Jeong, and N. Park, Nat. Commun. **7**, 13012 (2016).

[34] M. B. Muhlestein, C. F. Sieck, P. S. Wilson, and M. R. Haberman, Nat. Commun. **8**, 15625 (2017).

[35] C. F. Sieck, A. Alù, and M. R. Haberman, Phys. Rev. B **96**, 104303 (2017).

[36] J. Li, C. Shen, A. Díaz-Rubio, S. A. Tretyakov, and S. A. Cummer, Nat. Commun. **9**, 1342 (2018).

[37] L. Quan, Y. Ra'di, D. L. Sounas, and A. Alù, Phys. Rev. Lett. **120**, 254301 (2018).

[38] A. Diaz-Rubio and S. A. Tretyakov, Phys. Rev. B **96**, 125409 (2017).

[39] D. M. Pozar, *Microwave Engineering* (John Wiley & Sons, New York, 2009).

[40] A. Mostafazadeh, Phys. Rev. Lett. **102**, 220402 (2009).

[41] T.-Y. Huang, C. Shen, and Y. Jing, J. Acoust. Soc. Am. **140**, 908 (2016).

[42] F. Bongard, H. Lissek, and J. R. Mosig, Phys. Rev. B **82**, 094306 (2010).

[43] C. Shen, Y. Xie, N. Sui, W. Wang, S. A. Cummer, and Y. Jing, Phys. Rev. Lett. **115**, 254301 (2015).

[44] A. W. Leissa, Vibration of plates, NASA Report No. NASA SP-160 (Washington, DC, 1969).

[45] A. F. Seybert and D. F. Ross, J. Acoust. Soc. Am. **61**, 1362 (1977).

[46] Y. Xie, W. Wang, H. Chen, A. Konneker, B.-I. Popa, and S. A. Cummer, Nat. Commun. **5**, 5553 (2014).

[47] K. Ding, G. Ma, M. Xiao, Z. Q. Zhang, and C. T. Chan, Phys. Rev. X **6**, 021007 (2016).

[48] K. Ding, G. Ma, Z. Q. Zhang, and C. T. Chan, Phys. Rev. Lett. **121**, 085702 (2018).